ACS POLYMERS Au
AN OPEN ACCESS JOURNAL OF THE AMERICAN CHEMICAL SOCIETY

pubs.acs.org/polymerau
Article

Monitoring Protein Complexation with Polyphosphazene Polyelectrolyte Using Automated Dynamic Light Scattering Titration and Asymmetric Flow Field Flow Fractionation and Protein Recognition Immunoassay

Michael Lueckheide, Alexander Marin, Harichandra D. Tagad, Nicholas D. Posey, Vivek M. Prabhu,* and Alexander K. Andrianov*

Cite This: ACS Polym. Au 2023, 3, 354−364
Read Online

ACCESS | Metrics & More | Article Recommendations | Supporting Information

ABSTRACT: Polyphosphazenes represent a class of intrinsically flexible polyelectrolytes with potent immunoadjuvant activity, which is enabled through non-covalent self-assembly with antigenic proteins by charge complexation. The formation of supramolecular complexes between polyphosphazene adjuvant, poly[di-(carboxylatophenoxy)phosphazene] (PCPP), and a model vaccine antigen, hen egg lysozyme, was studied under physiological conditions using automated dynamic light scattering titration, asymmetric flow field flow fractionation (AF4), enzyme-linked immunosorbent assay (ELISA), and fluorescent quenching methods. Three regimes of self-assembly were observed covering complexation of PCPP with lysozyme in the nano-scale range, multi-chain complexes, and larger aggregates with complexes characterized by a maximum loading of over six hundred protein molecules per PCPP chain and dissociation constant in the micromolar range ($K_d = 7 \times 10^{-6}$ mol/L). The antigenicity of PCPP bound lysozyme, when compared to equivalent lysozyme solutions, was largely retained for all complexes, but observed a dramatic reduction for heavily aggregated systems. Routes to control the complexation regimes with elevated NaCl or KCl salt concentrations indicate ion-specific effects, such that more smaller-size complexes are present at higher NaCl, counterintuitive with respect to PCPP solubility arguments. While the order of mixing shows a prominent effect at lower stoichiometries of mixing, higher NaCl salt reduces the effect all together.

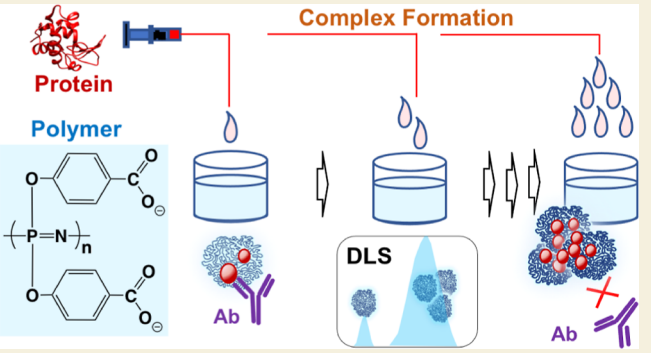

KEYWORDS: *polyphosphazenes, immunoadjuvants, protein−polymer complexes, self-assembly, dynamic light scattering, immunoassay*

INTRODUCTION

In achieving effective and long-lasting protection against infectious diseases, contemporary vaccines increasingly rely on the aid of immunoadjuvants and delivery systems, which are capable of augmenting and modulating the host immune response to vaccine antigen.[1−5] Although most of those systems traditionally include inorganic salts, emulsions, and small molecules, some of the alternative approaches encompass double-stranded RNAs poly(I/C), immune stimulating complexes (ISCOMs), and biodegradable polymers.[6−9] Among the latter is a water-soluble polyelectrolyte—poly[di-(carboxylatophenoxy)phosphazene] (PCPP), which realizes its potent immunoadjuvant effect in vivo via formation of physiologically stable complexes with antigenic proteins and accompanying immunostimulating action.[10,11] The self-assembly of PCPP with vaccine antigens is typically a spontaneous process leading to homogeneous water-soluble formulations and the properties of the resulting nano-sized supramolecular complexes can greatly affect their immunostimulating activity and in vivo performance.[12,13] It has been long established that the dimensions and biophysical characteristics of nanoparticulate vaccines can strongly affect their uptake by immunocompetent cells, lymphoid tissue, and as a result, influence magnitude and quality of the immune response.[14−18] Characterization of the size, structure, and solution behavior of complexes used in prophylactic and therapeutic vaccines is also essential to achieve regulatory approval. Therefore, the complexation behavior of PCPP with antigenic proteins in vaccine formulation is critical to understanding the mechanism

Received: February 17, 2023
Revised: March 31, 2023
Accepted: April 5, 2023
Published: April 21, 2023

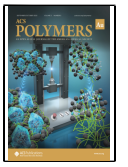

of action and developing the most advanced, safe, and potent formulations.

The formation of stable nano-sized polyelectrolyte-protein complexes are mediated by electrostatic interactions between net oppositely charged species. Experimental measurements and theoretical predictions show that such complexation criteria depend upon the ionic strength, polyelectrolyte charge density, pH-dependent protein surface charge density, and relative size characteristics, such as the radius of gyration of the polyelectrolyte and protein.[19] The stoichiometry of mixing plays an additional role in the stability of the complexes. Soluble complexes can transition to flocculation and macrophase separation (coacervation), or precipitation as shown in polyelectrolyte systems,[20−22] as well as with proteins.[19,23−25] Stable, soluble complexes with control of relevant particle size through molecular mass and charge stoichiometries below the point of charge neutralization, or phase separation that maintain protein function are critical in the heuristic design of formulations.

Hen egg lysozyme, a well-characterized protein that is commonly used as a model vaccine antigen,[26−28] forms intermolecular complexes with PCPP.[13,29,30] Moreover, in vivo studies have demonstrated that PCPP displayed a potent immunoadjuvant effect when formulated with hen egg lysozyme.[31] The isoelectric point of lysozyme is ≈11.1,[32,33] which leads to a net positive charge at physiological pH of 7.4. The chemical structure of PCPP shows two carboxylate groups per repeat unit making PCPP highly negatively charged. Therefore, PCPP-lysozyme formulations present an attractive model system for evaluating the mechanism of PCPP self-assembly and assessing potential applicability of diverse analytical techniques for the analysis of intermolecular interactions. The role of charge complexation as a mechanism for binding is certainly one explanation for binding between oppositely charged protein and polyelectrolyte, although dispersive interactions and solvation forces represent additional molecular level contributions to the overall interactions.[34] Molecular level effects such as protein charge heterogeneity and micro- and macrophase separation are also important in complex coacervates.[35] Aside from molecular mechanisms and a detailed evaluation of structure, the antigenicity of the protein informs about the accessibility of protein by antibodies—a key biological function of the complexes.

In the present study, we investigate the effects of lysozyme-to-PCPP stoichiometry, salt concentration, salt identity, and the order of addition of components on supramolecular complex formation. Dynamic light scattering (DLS), which is used in conjunction with an automated titration system capable of precise dosing of components, enables exploration of order-of-addition effects on characteristic size distributions. Asymmetric flow field flow fractionation (AF4) provides an analytical tool for quantitative estimation of complex composition and its dissociation constant. Binding interactions are also followed by quenching the intrinsic fluorescence of lysozyme, and the antigenicity of the bound protein was evaluated by enzyme-linked immunosorbent assay (ELISA). Here, we report three regimes of supramolecular assembly in lysozyme PCPP systems, which include nano-scale and aggregated complexes, prominent effect of order of component addition, micromolar range dissociation constant of the complex, ion-specific salt-effects, and remarkable maintenance of lysozyme antigenicity in aggregate-free assemblies.

MATERIALS AND METHODS

Materials

Lysozyme, NaCl-sodium chloride, KCl-potassium chloride (Sigma-Aldrich, Saint Louis, MO), and phosphate-buffered saline (PBS) pH 7.4 (Life Technologies, Carlsbad, CA) were used without further purification. Poly[di(carboxylatophenoxy)phosphazene] (PCPP) with a mass average molar mass of 800,000 g/mol was synthesized and characterized by size-exclusion chromatography and multi-angle laser light scattering as previously described.[36,37] The stock PCPP solution was originally prepared at 2 mg/mL in PBS and was stored at 4 °C when not in use. The PCPP stock solution was filtered with poly(vinylidene fluoride) (PVDF) Millex syringe filter units (EMD Millipore, Billerica, MA) with pore sizes of 0.22 μm after removal from cold storage and prior to subsequent dilutions (stability data for PCPP and lysozyme are shown in Tables S1 and S2). Protein and diluted PCPP solutions were prepared in PBS at pH 7.4 containing 137 mmol/L NaCl, or a 1x phosphate buffer containing 137 mmol/L KCl and 2.8 mmol/L NaCl. Filtered and deionized water with a resistivity of 18.2 MΩ cm^{-1} obtained from an Milli-Q apparatus was used throughout the study (effects of dilution and filtration on DLS data are shown in Tables S3 and S4). The model of lysozyme (protein databank entry 1DPX)[38] was rendered using Chimera software.[39]

Instrumentation

DLS measurements were performed with a Malvern Zetasizer Nano ZS (Malvern Instruments Ltd., Worcestershire, UK) using a 532 nm laser with data recorded and processed in Malvern Zetasizer Software 7.13. A Malvern MPT-2 autotitrator accessory was coupled to the Zetasizer and was controlled using the MPT-2 module within the Zetasizer software to enable titrations. A quartz flow cell with inlet and outlet tubing and adapters (Malvern Instruments Ltd., Worcestershire, UK) was used for titration measurements. Disposable polystyrene cuvettes with plastic caps were used for DLS measurements that were not part of a titration. Typically, 10 measurements on each sample were performed and the average size and size distribution from the general-purpose data analysis Malvern software was reported for automated titration measurements, but a cumulant analysis was also used in the case of single particle results such as protein and polymer.

DLS and ζ-Potential Characterization of PCPP, Lysozyme, and Complexes Thereof

The PCPP stock solution was diluted to 0.2 and 0.5 mg/mL in PBS, filtered through PVDF membranes with a pore size of 0.22 μm, and then studied by DLS at two angles, 173 and 12.8°, to characterize the polymer in the absence of protein. A lysozyme solution was prepared at 1 mg/mL in PBS and passed through a PVDF syringe filter unit with a pore size of 0.1 μm prior to characterization by DLS. To prepare complexes, PCPP stock solution was filtered through PVDF membranes with 0.22 μm pores and then diluted to 1 mg/mL in PBS. After dilution, 500 μL of the 1 mg/mL PCPP solution was filtered again through 0.22 μm pores directly into a clean polystyrene cuvette. Lysozyme solution (500 μL of 1 mg/mL) was filtered through 0.22 μm pore size PVDF membrane directly into the cuvette containing PCPP. The solution was mixed by pipetting up and down. Both solutions were thus mutually diluted to yield a final solution of complexes that was 0.5 mg/mL with respect to both PCPP and lysozyme. Due to the high molecular mass of the PCPP, the final concentration is near, but below the estimated overlap concentration ($c^* \approx 2$ mg/mL). The complex solution was characterized by DLS at two angles, 173 and 12.8°. The stability of complexes at multiple mole ratios was also evaluated via DLS at 173°. Samples were prepared at (5:1, 22:1, and 111:1) mole ratios of lysozyme to PCPP by the addition of 500 μL of filtered lysozyme solution at 0.09 mg/mL, 0.4 mg/mL, or 2 mg/mL, respectively, to 500 μL of filtered 1 mg/mL PCPP solution in a polystyrene cuvette. Similarly, additional mole ratios (2:1, 7:1, 56:1, and 560:1) were prepared by the equal volumes of mixing approach. Disposable, folded capillary ζ potential cells (Malvern DTS1070) were used in the ζ potential measurements.

https://doi.org/10.1021/acspolymersau.3c00006
ACS Polym. Au 2023, 3, 354−364

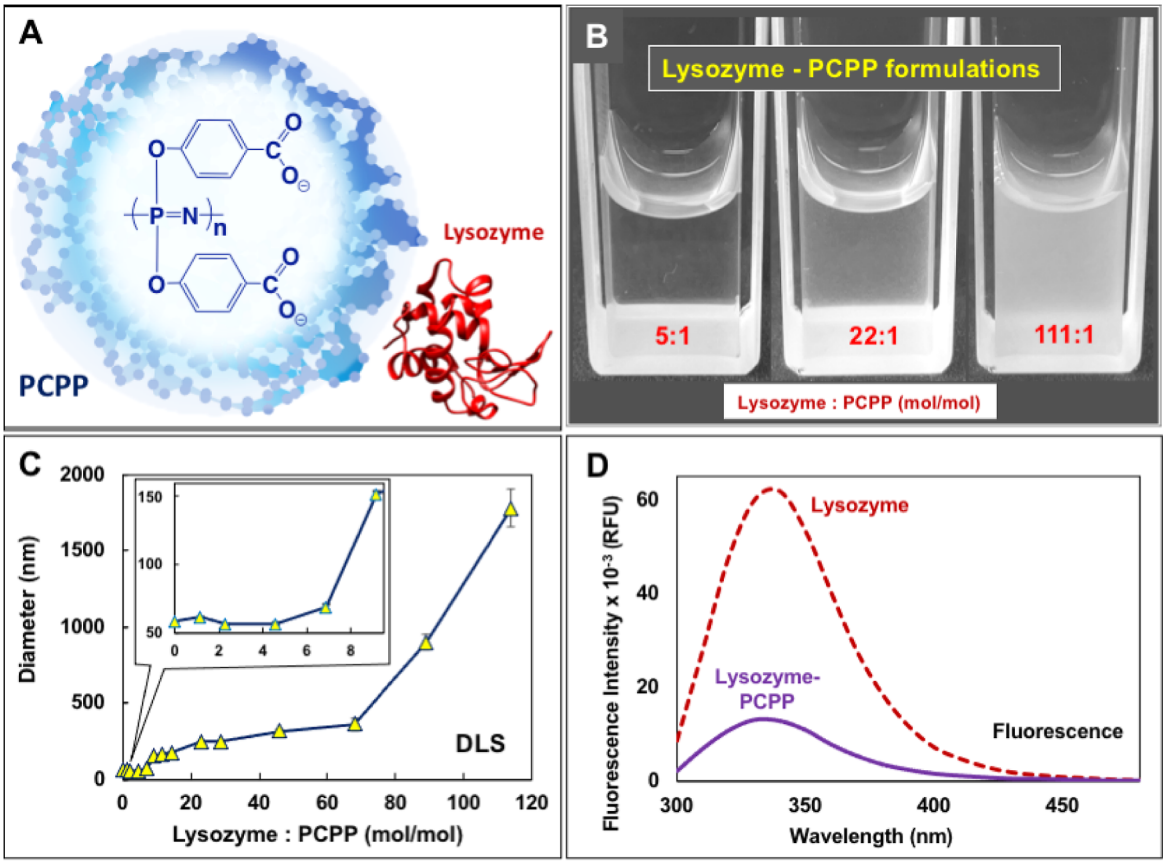

Figure 1. (A) Schematic presentation of PCPP and lysozyme; (B) photographs of lysozyme-PCPP formulations at various protein-to-polymer molar ratios (1 mg/mL PCPP, PBS, pH 7.4); (C) *z*-average hydrodynamic diameter of lysozyme-PCPP complexes as a function of molar ratio of components in the formulation (equal volume DLS method, 0.5 mg/mL PCPP, PBS pH 7.4, error bars- standard deviation, $n = 3$); (D) quenching of intrinsic fluorescence of lysozyme (red, dotted line) in a complex with PCPP (purple, solid line) (final concentrations are 0.3 mg/mL lysozyme, 0.2 mg/mL PCPP, in PBS pH 7.4, 250 nm excitation wavelength).

Automatic attenuation and voltage selection were used for all samples. Automated analysis was applied because of the high conductivity of the solution and yielded the mean particle mobility of the solution per run with the ζ potential values calculated using the Smoluchowski model provided by the Malvern software. The averaged and one standard deviation from three consecutive runs were reported.

Automated DLS Titrations with PCPP and Lysozyme

A Malvern MPT-2 autotitrator system, a Zetasizer Nano ZS, and a quartz flow cell were set up in conjunction to titrate PCPP with lysozyme, or to titrate lysozyme with PCPP, and to monitor each step of the titration with DLS. In general, the filtered solutions at 0.5 mg/mL were titrated with a 10 mg/mL solution of the opposite component that was filtered through 0.1 μm pore size PVDF syringe units. The titrant line was submerged in a plastic tube or reservoir containing 4−5 mL of the titrant solution, while the 5 mL analyte solution was stored in a separate reservoir. First, a peristaltic pump circulated the 5 mL of analyte solution through the lines to fill the quartz cell. Several slow filling cycles were completed to ensure elimination of air bubbles in the cell and lines. A separate pump dispensed the titrant solution in increments into the reservoir tube that contained a small Teflon-coated stir bar and analyte. Following each addition of titrant solution, a stir bar was used to mix the PCPP and lysozyme solution. The peristaltic pump then circulated the mixed solution through the lines and flow cell prior to each DLS measurement. This process was repeated automatically until the programmed end of the titration. Complexes were characterized by DLS at mole ratios of lysozyme to PCPP ranging from 22:1 to 330:1 in steps of 22 using 100 μL additions. The mass of each macromolecule, the molar mass of each macromolecule, and the number of charges per mole of macromolecule were used to compute how the mass, mole, and charge ratio changed throughout the titration. Diluted Hellmanex III cleaning solution (Hellma USA, Inc., Plainview, NY 11803) dissolved residual, precipitated complexes from the quartz flow cell cuvette, and basic aqueous solution (pH ≈ 9) was pumped through the lines and peristaltic pump to clean the system after each titration followed by excess deionized water. The non-invasive backscatter detection angle of 173° was reported for the automated titration DLS studies due to the shorter path length of laser light traveled through the sample cuvette, focusing lens that optimize the path length of the scattered light before reaching the detector close to the wall of the cuvettes, all of which reduces the effects of multiple scattering.[40,41]

Asymmetric Flow Field Flow Fractionation Analysis

The AF4 instrument (AF2000 AT, Postnova Analytics GmbH, Germany) was equipped with the PN7149 solvent organizer, PN7520 solvent degasser, PN1130 isocratic focus pump, PN1130 isocratic tip pump, AF2000 module with two cross flow pumps, AF2000MT channel with 350 μm spacer, mounted on PN5120 injection bracket, and SPD-20A Prominence UV/VIS detector. A regenerated cellulose membrane with a molecular mass cutoff of 10 kDa (Postnova, Germany) was used as a separation membrane, and PBS (filtered through 0.1 μm pore size) was employed as an eluent. The injection volume was 50 μL. The detailed instrument setup and elution programing are shown in Table S5. For quantitative analysis of lysozyme, the peak area in the range between 4.5 and 9.0 min, which corresponds to unbound protein was measured. The calibration (peak area vs lysozyme concentration) curve for the determination of unbound lysozyme and the recovery of lysozyme are shown in Figure S1.

https://doi.org/10.1021/acspolymersau.3c00006
ACS Polym. Au 2023, 3, 354−364

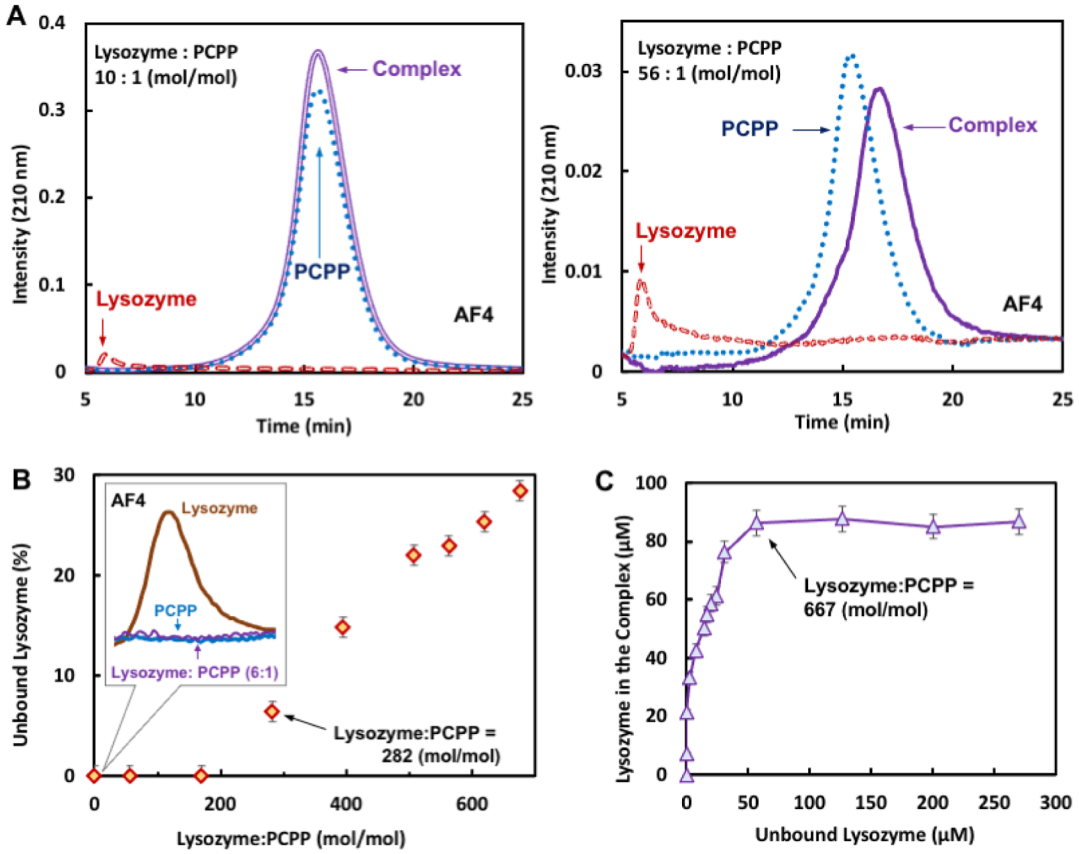

Figure 2. (A) Representative AF4 fractograms of lysozyme (red, dashed line), PCPP (blue, dotted line), and lysozyme-PCPP complex (purple, solid line) at different protein-to-polymer ratios (0.1 mg/mL PCPP, PBS, pH 7.4); (B) AF4 detected unbound lysozyme in formulations (error bars represent 1 standard deviation). The inset with a fragment of AF4 fractogram demonstrates disappearance of free lysozyme peak (brown, solid line; peak maximum—5.7 min) from lysozyme-PCPP formulation (6:1 molar ratio). (C) Isotherm of sorption for the lysozyme-PCPP system (error bars represent 1 standard deviation).

Enzyme-Linked Immunosorbent Assay Studies

The antigenicity of hen egg white lysozyme was evaluated using ELISA similarly to a previously described protocol.[26] The 96-well plate was coated overnight at 4 °C with 100 μL of 100 ng/mL rabbit anti-chicken egg lysozyme antibody (Rockland Immunochemicals, Inc., Pottstown, PA) in carbonate buffer (pH 9.2). The coating solution was removed, the plate was washed three times with PBS (pH 7.4), blocked by adding 300 μL/well of 1% BSA/0.05% Tween-20 in PBS (blocking buffer) for 1 h at 37 °C, and then washed four times with 0.05% Tween-20 in PBS. To prepare a calibration curve, 100 μL of lysozyme solution in blocking buffer [(5 to 100) μg/mL] was added to each well.

For the analysis, lysozyme formulations were diluted twofold with 2x blocking buffer, added to the plate (100 μL/well), incubated at 37 °C for 1 h, and then washed four times with 0.05% Tween-20 in PBS. Anti-lysozyme antibody (rabbit, anti-chicken, peroxidase conjugated—Rockland Immunochemicals, Inc., Pottstown, PA) in blocking buffer (500 ng/mL) was added (100 μL/well) and the plate was incubated at an ambient temperature for 1 h. The plate was washed as described above and the substrate—3,3′,5,5′-tetramethylbenzidine (MilliporeSigma, St. Louis, MO) was added (100 μL/well). The reaction was stopped after 20 min by adding 100 μL of 1 mol/L sulfuric acid to each well. The absorbance was read at 450 nm using Multiskan Spectrum Reader (Thermo Fisher Scientific, Waltham, MA). For the analysis of PCPP-containing lysozyme formulations, PCPP solution (25 μg/mL) in blocking buffer (100 μL/well) was subjected to the above treatments and was used as a background reference. All experiments were performed in triplicate.

RESULTS AND DISCUSSION

Physico-Chemical Characterization of Intermolecular Complexes between Lysozyme and PCPP

The well-established immunoadjuvant activity of PCPP (Figure 1A) has been directly linked to its ability to spontaneously self-assemble with antigenic proteins in aqueous solutions.[10] Interactions of PCPP with hen egg lysozyme are of particular interest as this protein is frequently employed as a model vaccine antigen,[26−28] spontaneously forms complexes with PCPP,[13,29,30] and demonstrates a dramatic increase in immunogenicity, when adjuvanted by PCPP in vivo.[31] Therefore, PCPP-lysozyme formulations present an attractive model system for evaluating the mechanism of PCPP self-assembly.

The existence and strength of intermolecular interactions in the PCPP-lysozyme system can be generally illustrated by the formation of formulations with noticeable turbidity, which occurs upon mixing of clear solutions of PCPP and lysozyme and progressively increases as the molar protein-to-polymer ratio rises (Figure 1B). DLS measurements displayed an increase in scattering intensity by orders of magnitude for the solution of complexes as compared to the separate solutions of PCPP and lysozyme (Figure S2A). Furthermore, scattering intensity at 12.8°, which is very low for PCPP alone, increases by orders of magnitude for its formulation with protein (Figure S2A). DLS size distribution profiles show that the hydrodynamic diameter of the complex is substantially larger than

https://doi.org/10.1021/acspolymersau.3c00006
ACS Polym. Au 2023, 3, 354−364

that of PCPP reaching the micron scale at a high protein-to-polymer mole ratio (Figure S2B). Autocorrelation functions (Figure S3A) and DLS profiles (Figure S3B) of lysozyme-PCPP complexes display a monomodal distribution with a polydispersity index ranging from 0.263 to 0.399 as the protein-to-polymer molar ratio increases from 7 to 89 with standard deviation not exceeding 5% for all samples (Table S6). Given the monodisperse complex size distribution, the *z*-average diameter, which is based on cumulant algorithm and provides "first-hand" information on the complex dimensions, was monitored according to recommendations on DLS reporting.[40,42] Overall, the *z*-average hydrodynamic diameter of the complex shows a gradual increase as the protein-to-polymer mole ratio rises, which was estimated on the basis of their molar masses: 800 kDa for PCPP versus 14.5 kDa for lysozyme (Figure 1C). Alternative representation of the size distribution, such as by volume or number, are not shown here due to the rather ill-defined structure of the complexes. The complexes are not solid particles with a well-defined refractive index, or low polydispersity micelles and therefore the intensity distributions do not rely on a particular model for converting into different weighted distributions. An in-depth analysis through combinations of multiple analytical methods would offer a more refined interpretation as with well-defined particles as reviewed by Cinar et al.[43] The large polydispersity may be expected by the nature of the complexation with polydisperse PCPP, which does not have a structure-driving mechanism such as a hydrophobic block that forms well-defined core−shell micelles in aqueous dispersed block copolymers.

The intrinsic fluorescence of lysozyme, which primarily originates from tryptophan residues,[44] has been extensively utilized to investigate interactions of this protein with numerous macromolecular and small molecule agents.[45−48] In particular, it was observed that macromolecules, such as dextran, can induce quenching of the fluorescence of lysozyme via influencing the local tryptophan environment without causing significant change in the global structure of the protein.[48] Fluorescence measurements indicated that PCPP was also effective in quenching the fluorescence of lysozyme, which independently confirmed the existence of protein−polymer interactions in the system (Figure 1D).

To independently confirm lysozyme binding to PCPP and determine the composition of intermolecular PCPP-lysozyme complexes, the AF4 method was applied. AF4 separates macromolecules and nanoparticles by their size with an analysis similar to size-exclusion chromatography, but allows characterization of analytes with dimensions up to the micron length scale.[49] The method was also successfully applied to quantitative analysis of polymer−protein complexes.[13,50,51] Figure 2A shows representative fractograms for formulations with low (10:1 mol/mol) and high (56:1 mol/mol) protein content. The formation of the complex can be monitored by the disappearance or decrease in the lysozyme peak (6 min) and increase in size and shift of the macromolecular PCPP peak (16.5 min) toward longer elution volumes. It was noted that the unbound lysozyme was detected in formulations that exceeded 282 (mol/mol) protein-to-polymer ratio (Figure 2B). An isotherm of protein binding by PCPP, which was calculated based on the amount of unbound lysozyme in the system detected by AF4, shows binding of up to 667 protein copies per PCPP chain (Figure 2C) with binding constant of $K_d = 7 \times 10^{-6}$ mol/L. The assessment of binding constant was conducted on the basis of a simplified binding model by determining concentration of lysozyme at a half-saturation of PCPP.[52] The formation of such multimeric complexes with PCPP acting as a host for protein ligands is expected due to large molar mass disparity between the two macromolecules (800 kDa for PCPP vs 14.5 kDa for lysozyme).

The inset in Figure 1C shows that the hydrodynamic diameter of PCPP remains unchanged upon addition of lysozyme until the molar protein-to-polymer ratio reaches values in excess of seven. The presence of protein-polymer association in such systems was investigated by AF4 and fluorescence analysis. The inset in Figure 2B shows that the free lysozyme peak (peak maximum—5.7 min) in an AF4 fractogram disappears upon mixing with PCPP at 6:1 protein-to-polymer molar ratio. This indicates lysozyme-PCPP binding in a formulation, which is characterized by hydrodynamic diameter, is identical to that of PCPP (Figure 1C, inset). Furthermore, quenching of lysozyme fluorescence by PCPP, which is observed in a broad range of molar ratios (Figure S4), and indicates lysozyme-PCPP interactions, is also evident for the low-molar ratios range (Figure S4D). Taken together, AF4 and fluorescence results suggest the formation of lysozyme-PCPP complexes detected by DLS in the nano-scale range (less than 100 nm).

Automated DLS Titration of PCPP with Lysozyme

Studying the formation of protein-polymer complexes by varying the ratios of components using titrimetric techniques provides valuable information on the mechanism of self-assembly.[53] Figure 3 shows the results of an automated DLS titration, whereby lysozyme was added to PCPP solution in the range of 22:1 to 111:1 protein-to-polymer molar ratios. As seen from the figure, the addition of protein to polymer solution results in a bimodal size distribution when the molar excess of lysozyme is 22 protein molecules per polymer chain. In this formulation, PCPP chains appear to co-exist with the complexes, which exceeds the size of the polymer by

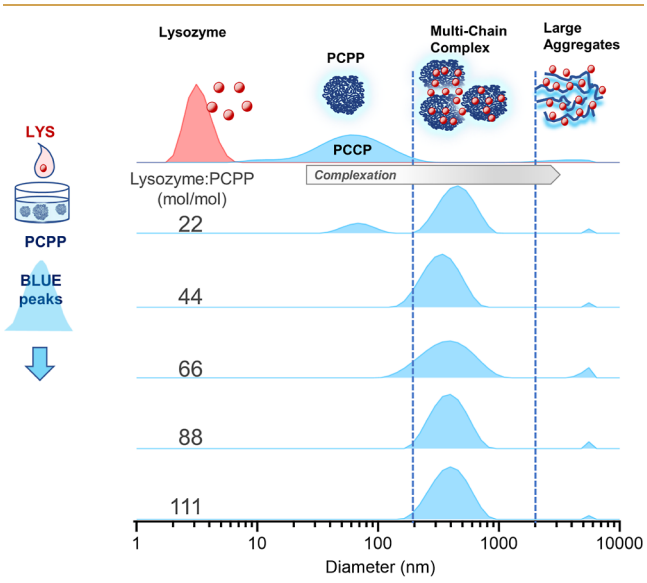

Figure 3. Representative results from an automated titration of PCPP with lysozyme showing an increase in the size of the hydrodynamic size distribution of PCPP as lysozyme was added incrementally. The distributions are vertically shifted for clarity with an arbitrary *y*-axis intensity (%) scale.

https://doi.org/10.1021/acspolymersau.3c00006
ACS Polym. Au 2023, 3, 354−364

approximately a factor of 8 (z-averages: 400 and 54 nm, correspondingly). Remarkably, no intermediate size complexes are formed. Furthermore, at a higher protein-to-polymer molar ratios, from 44:1 to 111:1, unimodal size distribution is observed with no apparent increase in the hydrodynamic diameter of the complex.

The ζ potentials of complexes prepared manually through pipette mixing of equal volumes of lysozyme added to PCPP at lysozyme/PCPP mole ratios of 22:1 and 111:1 were measured to be -29.5 ± 2.3 and -25.5 ± 2.7 mV, respectively. These demonstrate the overall negative charge of the complexes and explain the absence of further aggregation and precipitation under these conditions as resulting from stabilization due to electrostatic repulsions. As a point of reference, the ζ potential for 1 mg/mL of PCPP in the PBS buffer was -29.6 ± 0.9 mV showing a highly charged polyelectrolyte. The formation of micrometer size aggregates at a higher excess of the protein (Figure S6) decreases the stability. The net negative charges on these complexes also indicate that coacervation (macro-phase separation) is not occurring here. At a lysozyme/PCPP mole ratio of 600:1, the ζ potential was measured to be $\approx$4 mV, and the complexes ultimately precipitated within a few minutes, showing that a large excess of lysozyme can create complexes large enough to desolvate. An example of the kinetic stability of the complexes up to 7 days after mixing for 7:1 (Figure S7) and more than 24 h for 56:1 (Figure S8) is consistent with the magnitude of ζ potential that indicates stability.

The above results confirm the formation of the interpolymer lysozyme-PCPP complex with multiple protein ligands bound to the polymer. Interestingly, the data indicates that the polymer-complex transition occurs without a gradual increase in the size of the complex. Instead, it is realized through the co-existence of two populations with discretely different dimensions. An eight-fold difference between z-average hydrodynamic diameters suggests the presence of polymer or multi-chain complexes involving several PCPP chains. The multi-chain complex maintains its dimensions in a relatively broad range of protein-to-polymer ratios provided that negative charges of PCPP are in excess. The formation of supramolecular assemblies that contain several PCPP chains can be somewhat anticipated as lysozyme contains multiple positive charges that may act as an electrostatic cross-linker for PCPP in the way other multivalent ions may induce physical cross-links or gelation.[54,55] At sufficiently high protein concentration, the stability of the multi-chain complexes reduces due to a charge reversal and colloidal instability. Such electrostatic effects on stability naturally poses the question if the order of addition influences the general formation of complexes of different dimensions.

Automated DLS Titration of Lysozyme with PCPP

The order of addition of PCPP and lysozyme during complex formation significantly affects the resulting complexes, as shown in Figure 4. Complexes formed by the addition of PCPP into lysozyme monotonically increase in hydrodynamic diameter as PCPP is added and the lysozyme/PCPP mole ratio steps from 111 to 22. At a mole ratio of 66, a mixture of free PCPP and complexes appears that persists as more PCPP is added. When lysozyme is added to PCPP, the resulting complexes instead maintain approximately the same mean hydrodynamic diameter and have size distributions that increase in width as more lysozyme is added. At a mole ratio

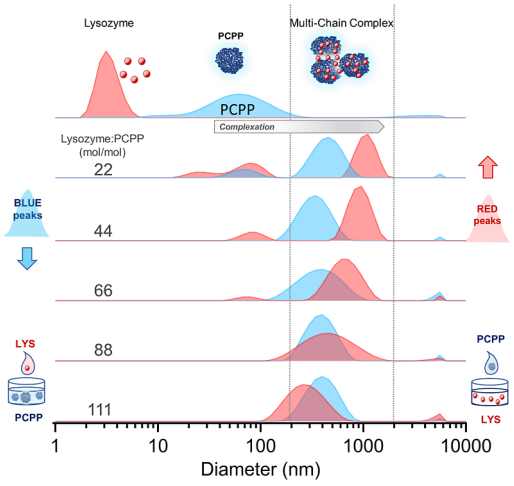

Figure 4. Representative results of automated titrations of PCPP with lysozyme (blue peaks) and lysozyme with PCPP (red peaks) encompassing lysozyme/PCPP mole ratios between 22 and 111. They show significant differences between the size distributions of the resulting complexes based on the order of addition of the components. The distributions are vertically shifted for clarity with an arbitrary y-axis intensity (%) scale.

of 308:1, free lysozyme starts to appear that persists at higher mole ratios. The complexation process proceeds and observing free lysozyme implies PCPP has accessible anionic binding sites even before molar ratios where charge neutralization were to occur. The difference in multi-chain complex size and distribution correlates with an order-of-addition-dependent polyelectrolyte complexation[56,57] behavior that emphasizes the need for consistent complex preparation procedures while offering a degree of flexibility with respect to the desired product. Such phase behavior may provide insights into consistent preparation of biopharmaceutical formulations.

DLS measurements taken immediately after mixing the components revealed slow modes in the autocorrelation function that indicate a presence of large aggregates. Subsequent measurements show that the autocorrelation functions smoothed over time, suggesting these larger aggregates dispersed into smaller populations. This suggests a temporal character of the observed phenomenon and annealing of lysozyme-PCPP complexes mediated via ion exchange interactions.

Salt Effects on Lysozyme-PCPP Complexes

Due to the highly charged nature of PCPP and importance of electrostatics to the stability of complexes, the effect of salt on the formation of complexes was investigated. In this respect, PCPP is known to be soluble in a broad range of KCl concentrations, while, NaCl and sodium ions, specifically, are known to cause PCPP to form coacervate phases and phase separate at concentrations exceeding 350 mmol/L.[36,54] This introduced an ion-specific effect on lysozyme/PCPP complex-ation that can be tested by changing the salt concentrations. Automated titrations were conducted as before with samples prepared either at (137 or 350) mmol/L of NaCl or KCl in 10 mmol/L phosphate buffer with the order of addition of lysozyme into PCPP solutions.

High concentrations of both salts, which correspond to a three-fold increase over ionic strength of PBS (three-fold higher than at near physiological conditions), do not prevent formation of complexes (Figure 5). High salt concentration

https://doi.org/10.1021/acspolymersau.3c00006
ACS Polym. Au 2023, 3, 354−364

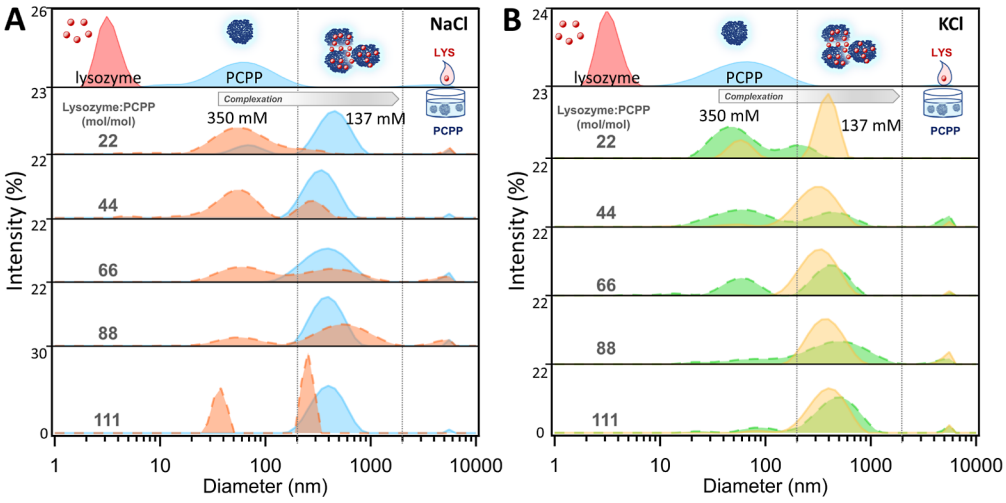

Figure 5. Effect of low (137 mM, blue and yellow −) and high (350 mM, orange and green, ---) concentrations of (A) sodium chloride and (B) potassium chloride on the formation of complexes shown for lysozyme/PCPP mole ratios from 22 to 111. The distributions that are vertically shifted for clarity range from 0% to the full-scale value provided on the common intensity (%) axis.

also mitigates the effect of the order of addition of components by disfavoring the formation of multi-chain complexes as shown in Figures 5A and 6 for NaCl.

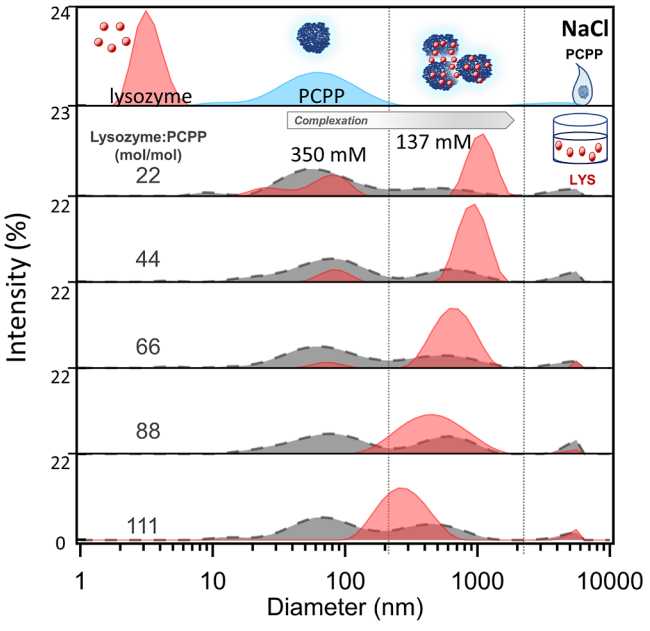

Figure 6. High concentration of 350 mmol/L NaCl (black, ---) sodium chloride promotes the formation of complex populations for PCPP into lysozyme vs 137 mmol/L NaCl (red, −) shown for lysozyme/PCPP mole ratios from 22 to 111. The distributions that are vertically shifted for clarity range from 0% to the full-scale value provided on the common intensity (%) axis.

Although the above DLS results provide direct evidence only for the formation of multi-chain complexes, AF4 data in Figure 7A shows no free lysozyme is present at a 5.7:1 mole ratio sample at 350 mmol/L NaCl. The lysozyme peak disappears after PCPP is added, which confirms that electrostatic interactions at low protein-to-polymer ratios are not suppressed by increased salt concentration, and that complexes with smaller overall dimensions form under those conditions. Fluorescence data in Figure 7B show the quenching of lysozyme fluorescence when PCPP is added, further confirming the incorporation of lysozyme into complexes. These findings are important because of the widespread concerns about inherent instability of non-covalently assembled supramolecular systems in the presence of salts potentially limiting their utility as drug delivery systems in vivo.[58−60]

Higher salt concentrations favor the formation of complex populations with smaller overall dimensions, such that sodium chloride appears to prevent aggregation more effectively than potassium chloride. Figure 5 shows larger populations of nanoscale complexes at 350 mmol/L NaCl than at 350 mmol/L KCl, which is consistent with the higher affinity of sodium ions to PCPP. Since multi-chain aggregation may not be desirable for many pharmaceutical applications, the results may offer a practical approach to formulation control via modulation of salt concentration and composition.

ELISA Illustrates Correlations of Antigenic Activity to Regimes of Complexes

Functionality of lysozyme-PCPP complexes at varying protein loadings was evaluated by measuring antigenicity of lysozyme using sandwich ELISA. The ability of lysozyme in the complex to interact with both capturing and detecting antibody in the assay at a low protein load (complexes with smaller dimensions) was practically identical to that of unbound lysozyme, which is evident from the analysis of initial stages of both curves (Figure 8A). Nevertheless, the deviation of the standard curve for the complex from the free lysozyme becomes increasingly noticeable as the load of lysozyme rises. As the complex reaches its aggregated stage, almost half of antigenicity is lost.

The above results indicate that lysozyme-PCPP complexes enable effective display of lysozyme and the availability of protein to both capturing antibody on the plate and detecting conjugate antibody in solution remains unlimited. This is schematically represented in Figure 8B (top and middle sections). The situation changes when the complex is converted to its aggregated state at high protein loading (bottom part of the same figure). Since efficient display of antigenic proteins is one of the key features of polyphosphazene immunoadjuvants and vaccine delivery vehicles,[10,13] these findings demonstrate the existence of strong relationship

https://doi.org/10.1021/acspolymersau.3c00006
ACS Polym. Au 2023, 3, 354−364

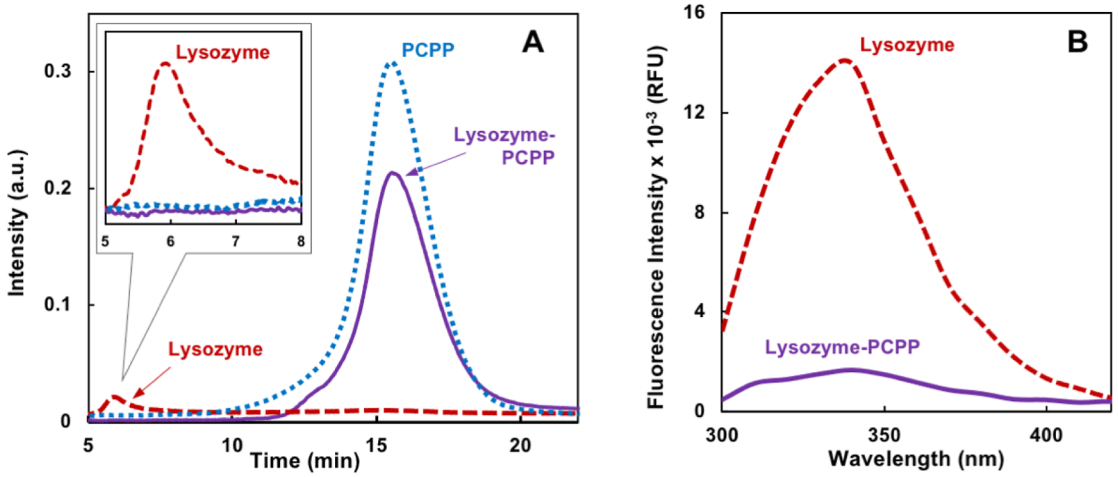

Figure 7. (A) AF4 fractograms of lysozyme (red, dashed line), PCPP (blue, dotted line), and the lysozyme-PCPP complex (purple, solid line) prepared as 0.1 mg/mL lysozyme mixed into 1.0 mg/mL PCPP (5.7:1 protein-to-polymer molar ratio) in the presence of 350 mmol/L NaCl at pH 7.4; (B) fluorescence profiles showing quenching of lysozyme fluorescence in the same complex (280 nm excitation, 350 mmol/L NaCl, pH 7.4).

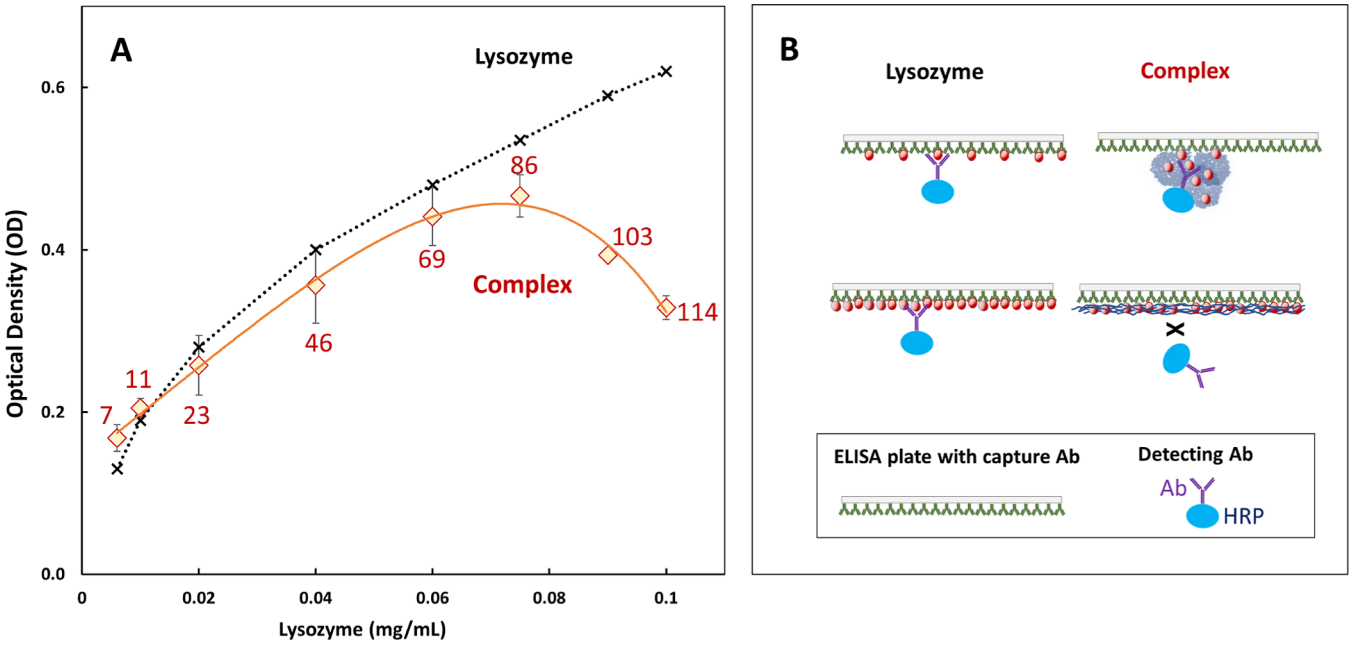

Figure 8. (A) ELISA standard curves for lysozyme (black, dotted line) and lysozyme-PCPP complexes (red, solid line), numbers (7−114) represent lysozyme-to-PCPP molar ratios (results are in triplicates and error bars (uncertainties) represent one standard deviation); (B) schematic presentation illustrating interactions of free lysozyme and lysozyme-PCPP complexes with ELISA plate containing capture antibody (Ab) and detecting Ab conjugated with horseradish peroxidase (HRP) in sandwich ELISA assay. As concentration of lysozyme increases (from top to bottom), interactions of detecting antibody with lysozyme in the complex are impeded for high protein load complex.

between biological functionality of PCPP and conformational state of the complex. This in turn, emphasizes the need for conducting comprehensive physico-chemical characterization of polyphosphazene adjuvanted vaccine formulations in order to understand the mechanism of action in those systems.

CONCLUSIONS

The PCPP model system formulated with lysozyme exhibits three regimes of complex formation that are a function of the mole ratio of mixing, order of addition of components, and salt concentration. Such a phase behavior was measured by automated DLS titrations and interpreted from analysis of the size distribution attributed to complexes characterized with overall chain dimensions of PCPP and multi-chain complexes of finite size, and lastly, large insoluble aggregates.

The relative population of complexes characterized by nano-scale dimensions and multichain-complexes depend upon the order of addition with the effect reduced at 111:1 mole ratio of lysozyme: PCPP. Lower mole ratios observe both complexes with smaller overall dimensions and multi-chain complexes. This effect was reduced by increasing the salt concentration from 137 to 350 mM, where a larger fraction of nano-scale complexes appears. In this case, there is an ion-specific effect where NaCl is more effective to reduce the multi-chain aggregates than KCl, while not compromising the ability of PCPP to bind lysozyme as shown by AF4 fractograms and fluorescence quenching. Even though electrostatic stabilization

https://doi.org/10.1021/acspolymersau.3c00006
ACS Polym. Au 2023, 3, 354−364

of the complexes takes place as measured by negative ζ-potentials, the excess salt, double that of the 1xPBS solution, does not reduce the stability or displace the protein. Therefore, salt type and concentration provide reasonable methods to modify formulations.

The multiple binding regimes between protein and PCPP illustrate an interplay of the high molecular mass PCPP acting as a host for the protein, while not disrupting the accessibility of its protein epitopes. The lysozyme-PCPP complexes showed equivalent antigenicity as free lysozyme as tested by an ELISA assays. This result observes that lysozyme remains displayed and accessible to antibodies within the high molecular mass PCPP chains. Importantly, the regime with large aggregates suppress antigenicity of lysozyme as tested by ELISA. Automated titration DLS combined with AF4 provides a means to assess complexation behavior. Such combinations of physicochemical measurements and biophysical assays are necessary to connect fundamentals to function.

■ ASSOCIATED CONTENT

Data Availability Statement

Raw or processed data files required for reproducing results will be made available upon reasonable request.

Supporting Information

The Supporting Information is available free of charge at https://pubs.acs.org/doi/10.1021/acspolymersau.3c00006.

Derived count rates as a measure of light scattering intensity; DLS profiles of PCPP and lysozyme-PCPP complexes at different protein-to-polymer mass ratios (w/w); quenching of lysozyme fluorescence by PCPP; example DLS profiles of lysozyme-PCPP complexes at different protein-to-polymer mass ratios (w/w) showing multiple modes for mixing PCPP into lysozyme; effects of storage time, stability of lysozyme, and dilution on the hydrodynamic diameter of PCPP and lysozyme; and AF4 instrumental setup and elution details (PDF)

■ AUTHOR INFORMATION

Corresponding Authors

Vivek M. Prabhu − *Materials Science and Engineering Division, Material Measurement Laboratory, National Institute of Standards and Technology, Gaithersburg, Maryland 20899, United States;* orcid.org/0000-0001-8790-9521; Email: vprabhu@nist.gov

Alexander K. Andrianov − *Institute for Bioscience and Biotechnology Research, University of Maryland, Rockville, Maryland 20850, United States;* orcid.org/0000-0001-6186-6156; Email: aandrianov@umd.edu

Authors

Michael Lueckheide − *Materials Science and Engineering Division, Material Measurement Laboratory, National Institute of Standards and Technology, Gaithersburg, Maryland 20899, United States*

Alexander Marin − *Institute for Bioscience and Biotechnology Research, University of Maryland, Rockville, Maryland 20850, United States*

Harichandra D. Tagad − *Institute for Bioscience and Biotechnology Research, University of Maryland, Rockville, Maryland 20850, United States*

Nicholas D. Posey − *Materials Science and Engineering Division, Material Measurement Laboratory, National Institute of Standards and Technology, Gaithersburg, Maryland 20899, United States;* orcid.org/0000-0001-9702-7960

Complete contact information is available at: https://pubs.acs.org/10.1021/acspolymersau.3c00006

Author Contributions

The manuscript was written through contributions of all authors. All authors have given approval to the final version of the manuscript. M.L. and A.M. are equal contributing first authors.

Notes

The authors declare no competing financial interest.

■ ACKNOWLEDGMENTS

M.L., N.D.P., and V.M.P. acknowledge partial support from the NIST Materials Genome Initiative and M.L. and N.D.P. acknowledge partial support from the NIST National Research Council Postdoctoral Research Associateship Program. This work was also supported in part by the National Institutes of Health Grant R01AI132213 (A.K.A.) and the National Science Foundation under Award DMR-1808531 (A.K.A.). Official contribution of the National Institute of Standards and Technology; not subject to copyright in the United States.

■ ABBREVIATIONS

PCPP	poly[di(carboxylatophenoxy)phosphazene]
PBS	phosphate-buffered saline
PVDF	poly(vinylidene fluoride)
DLS	dynamic light scattering
AF4	asymmetric flow field flow fractionation
ELISA	enzyme-linked immunosorbent assay
K_d	dissociation constant
ISCOMs	immune stimulating complexes

■ REFERENCES

(1) Rappuoli, R.; Pizza, M.; Del Giudice, G.; De Gregorio, E. Vaccines, new opportunities for a new society. *Proc. Natl. Acad. Sci. U.S.A.* **2014**, *111*, 12288−12293.

(2) Del Giudice, G.; Rappuoli, R.; Didierlaurent, A. M. Correlates of adjuvanticity: A review on adjuvants in licensed vaccines. *Semin. Immunol.* **2018**, *39*, 14−21.

(3) Reed, S. G.; Orr, M. T.; Fox, C. B. Key roles of adjuvants in modern vaccines. *Nat. Med.* **2013**, *19*, 1597−1608.

(4) Nanishi, E.; Dowling, D. J.; Levy, O. Toward precision adjuvants: optimizing science and safety. *Curr. Opin. Pediatr.* **2020**, *32*, 125−138.

(5) Brito, L. A.; Malyala, P.; O'Hagan, D. T. Vaccine adjuvant formulations: A pharmaceutical perspective. *Semin. Immunol.* **2013**, *25*, 130−145.

(6) Matsumoto, M.; Seya, T. TLR3: Interferon induction by double-stranded RNA including poly(I:C). *Adv. Drug Delivery Rev.* **2008**, *60*, 805−812.

(7) Pearse, M. J.; Drane, D. ISCOMATRIX adjuvant for antigen delivery. *Adv. Drug Delivery Rev.* **2005**, *57*, 465−474.

(8) Powell, B. S.; Andrianov, A. K.; Fusco, P. C. Polyionic vaccine adjuvants: another look at aluminum salts and polyelectrolytes. *Clin. Exp. Vaccine Res.* **2015**, *4*, 23−45.

(9) Jain, S.; O'Hagan, D. T.; Singh, M. The long-term potential of biodegradable poly(lactideco-glycolide) microparticles as the next-generation vaccine adjuvant. *Expert Rev. Vaccines* **2011**, *10*, 1731−1742.

(10) Andrianov, A. K.; Langer, R. Polyphosphazene immunoadjuvants: Historical perspective and recent advances. *J. Controlled Release* **2021**, *329*, 299−315.
(11) Magiri, R.; Mutwiri, G.; Wilson, H. L. Recent advances in experimental polyphosphazene adjuvants and their mechanisms of action. *Cell Tissue Res.* **2018**, *374*, 465−471.
(12) Andrianov, A. K.; Marin, A.; Roberts, B. E. Polyphosphazene polyelectrolytes: A link between the formation of noncovalent complexes with antigenic proteins and immunostimulating activity. *Biomacromolecules* **2005**, *6*, 1375−1379.
(13) Andrianov, A. K.; Marin, A.; Fuerst, T. R. Molecular-Level Interactions of Polyphosphazene Immunoadjuvants and Their Potential Role in Antigen Presentation and Cell Stimulation. *Biomacromolecules* **2016**, *17*, 3732−3742.
(14) Foged, C.; Brodin, B.; Frokjaer, S.; Sundblad, A. Particle size and surface charge affect particle uptake by human dendritic cells in an in vitro model. *Int. J. Pharm.* **2005**, *298*, 315−322.
(15) Kanchan, V.; Panda, A. K. Interactions of antigen-loaded polylactide particles with macrophages and their correlation with the immune response. *Biomaterials* **2007**, *28*, 5344−5357.
(16) Rungrojcharoenkit, K.; Sunintaboon, P.; Ellison, D.; Macareo, L.; Midoeng, P.; Chaisuwirat, P.; Fernandez, S.; Ubol, S. Development of an adjuvanted nanoparticle vaccine against influenza virus, an in vitro study. *PLoS One* **2020**, *15*, No. e0237218.
(17) Stano, A.; Nembrini, C.; Swartz, M. A.; Hubbell, J. A.; Simeoni, E. Nanoparticle size influences the magnitude and quality of mucosal immune responses after intranasal immunization. *Vaccine* **2012**, *30*, 7541−7546.
(18) Mottram, P. L.; Leong, D.; Crimeen-Irwin, B.; Gloster, S.; Xiang, S. D.; Meanger, J.; Ghildyal, R.; Vardaxis, N.; Plebanski, M. Type 1 and 2 Immunity Following Vaccination Is Influenced by Nanoparticle Size: Formulation of a Model Vaccine for Respiratory Syncytial Virus. *Mol. Pharmaceutics* **2007**, *4*, 73−84.
(19) Comert, F.; Xu, A. Y.; Madro, S. P.; Liadinskaia, V.; Dubin, P. L. The so-called critical condition for polyelectrolyte-colloid complex formation. *J. Chem. Phys.* **2018**, *149*, 163321.
(20) Pogodina, N. V.; Tsvetkov, N. V. Structure and Dynamics of the Polyelectrolyte Complex Formation. *Macromolecules* **1997**, *30*, 4897−4904.
(21) Dautzenberg, H.; Hartmann, J.; Grunewald, S.; Brand, F. Stoichiometry and structure of polyelectrolyte complex particles in diluted solutions. *Ber. Bunsenges. Phys. Chem.* **1996**, *100*, 1024−1032.
(22) Dautzenberg, H. Polyelectrolyte Complex Formation in Highly Aggregating Systems. 1. Effect of Salt: Polyelectrolyte Complex Formation in the Presence of NaCl. *Macromolecules* **1997**, *30*, 7810−7815.
(23) Cummings, C. S.; Obermeyer, A. C. Phase Separation Behavior of Supercharged Proteins and Polyelectrolytes. *Biochemistry* **2018**, *57*, 314−323.
(24) Comert, F.; Malanowski, A. J.; Azarikia, F.; Dubin, P. L. Coacervation and precipitation in polysaccharide−protein systems. *Soft Matter* **2016**, *12*, 4154−4161.
(25) Comert, F.; Dubin, P. L. Liquid-liquid and liquid-solid phase separation in protein-polyelectrolyte systems. *Adv. Colloid Interface Sci.* **2017**, *239*, 213−217.
(26) Romero Méndez, I. Z.; Shi, Y.; HogenEsch, H.; Hem, S. L. Potentiation of the immune response to non-adsorbed antigens by aluminum-containing adjuvants. *Vaccine* **2007**, *25*, 825−833.
(27) Temchura, V. V.; Kozlova, D.; Sokolova, V.; Überla, K.; Epple, M. Targeting and activation of antigen-specific B-cells by calcium phosphate nanoparticles loaded with protein antigen. *Biomaterials* **2014**, *35*, 6098−6105.
(28) Akiba, H.; Tamura, H.; Kiyoshi, M.; Yanaka, S.; Sugase, K.; Caaveiro, J. M. M.; Tsumoto, K. Structural and thermodynamic basis for the recognition of the substrate-binding cleft on hen egg lysozyme by a single-domain antibody. *Sci. Rep.* **2019**, *9*, 15481.
(29) Andrianov, A. K.; Marin, A.; Deng, J.; Fuerst, T. R. Protein-loaded soluble and nanoparticulate formulations of ionic polyphosphazenes and their interactions on molecular and cellular levels. *Mater. Sci. Eng. C* **2020**, *106*, 110179.
(30) Burova, T. V.; Grinberg, N. V.; Dubovik, A. S.; Olenichenko, E. A.; Orlov, V. N.; Grinberg, V. Y. Interpolyelectrolyte complexes of lysozyme with short poly[di(carboxylatophenoxy)phosphazene]. Binding energetics and protein conformational stability. *Polymer* **2017**, *108*, 97−104.
(31) Kovacs-Nolan, J.; Mapletoft, J. W.; Latimer, L.; Babiuk, L. A.; Hurk, S. v. D. L.-v. d. CpG oligonucleotide, host defense peptide and polyphosphazene act synergistically, inducing long-lasting, balanced immune responses in cattle. *Vaccine* **2009**, *27*, 2048−2054.
(32) Kuehner, D. E.; Engmann, J.; Fergg, F.; Wernick, M.; Blanch, H. W.; Prausnitz, J. M. Lysozyme Net Charge and Ion Binding in Concentrated Aqueous Electrolyte Solutions. *J. Phys.Chem. B* **1999**, *103*, 1368−1374.
(33) Haynes, C. A.; Sliwinsky, E.; Norde, W. Structural and Electrostatic Properties of Globular Proteins at a Polystyrene-Water Interface. *J. Colloid Interface Sci.* **1994**, *164*, 394−409.
(34) Israelachvili, J. N. *Intermolecular and Surface Forces*; Elsevier, 2011.
(35) Horn, J. M.; Kapelner, R. A.; Obermeyer, A. C. Macro- and Microphase Separated Protein-Polyelectrolyte Complexes: Design Parameters and Current Progress. *Polymers* **2019**, *11*, 578.
(36) Andrianov, A. K.; Svirkin, Y. Y.; LeGolvan, M. P. Synthesis and biologically relevant properties of polyphosphazene polyacids. *Biomacromolecules* **2004**, *5*, 1999−2006.
(37) Andrianov, A. K.; Le Golvan, M. P. Characterization of poly[di(carboxylatophenoxy)-phosphazene] by an aqueous gel permeation chromatography. *J. Appl. Polym. Sci.* **1996**, *60*, 2289−2295.
(38) Weiss, M. S.; Palm, G. J.; Hilgenfeld, R. Crystallization, structure solution and refinement of hen egg-white lysozyme at pH 8.0 in the presence of MPD. *Acta Crystallogr.* **2000**, *56*, 952−958.
(39) Pettersen, E. F.; Goddard, T. D.; Huang, C. C.; Couch, G. S.; Greenblatt, D. M.; Meng, E. C.; Ferrin, T. E. UCSF Chimera—A visualization system for exploratory research and analysis. *J. Comput. Chem.* **2004**, *25*, 1605−1612.
(40) Bhattacharjee, S. DLS and zeta potential − What they are and what they are not? *J. Controlled Release* **2016**, *235*, 337−351.
(41) *Malvern Manual, Zetasizer Nano User Manual*; Malvern Instruments Ltd: Worcestershire, United Kingdom, 2010; Vol. *Man0317* Issue 5.0, August 2009.
(42) Stetefeld, J.; McKenna, S. A.; Patel, T. R. Dynamic light scattering: a practical guide and applications in biomedical sciences. *Biophys. Rev.* **2016**, *8*, 409−427.
(43) Cinar, G.; Solomun, J. I.; Mapfumo, P.; Traeger, A.; Nischang, I. Nanoparticle sizing in the field of nanomedicine: Power of an analytical ultracentrifuge. *Anal. Chim. Acta* **2022**, *1205*, 339741.
(44) Imoto, T.; Forster, L. S.; Rupley, J. A.; Tanaka, F. Fluorescence of Lysozyme: Emissions from Tryptophan Residues 62 and 108 and Energy Migration. *Proc. Natl. Acad. Sci. U.S.A.* **1972**, *69*, 1151−1155.
(45) Ding, F.; Zhao, G.; Huang, J.; Sun, Y.; Zhang, L. Fluorescence spectroscopic investigation of the interaction between chloramphenicol and lysozyme. *Eur. J. Med. Chem.* **2009**, *44*, 4083−4089.
(46) Crouse, H. F.; Potoma, J.; Nejrabi, F.; Snyder, D. L.; Chohan, B. S.; Basu, S. Quenching of tryptophan fluorescence in various proteins by a series of small nickel complexes. *Dalton Trans.* **2012**, *41*, 2720−2731.
(47) Revathi, R.; Rameshkumar, A.; Sivasudha, T. Spectroscopic investigations on the interactions of AgTiO2 nanoparticles with lysozyme and its influence on the binding of lysozyme with drug molecule. *Spectrochim. Acta, Part A* **2016**, *152*, 192−198.
(48) Singh, P.; Chowdhury, P. K. Unravelling the Intricacy of the Crowded Environment through Tryptophan Quenching in Lysozyme. *J. Phys. Chem. B* **2017**, *121*, 4687−4699.
(49) Messaud, F. A.; Sanderson, R. D.; Runyon, J. R.; Otte, T.; Pasch, H.; Williams, S. K. R. An overview on field-flow fractionation techniques and their applications in the separation and characterization of polymers. *Prog. Polym. Sci.* **2009**, *34*, 351−368.

https://doi.org/10.1021/acspolymersau.3c00006
ACS Polym. Au 2023, 3, 354−364

(50) Boye, S.; Ennen, F.; Scharfenberg, L.; Appelhans, D.; Nilsson, L.; Lederer, A. From 1D Rods to 3D Networks: A Biohybrid Topological Diversity Investigated by Asymmetrical Flow Field-Flow Fractionation. *Macromolecules* **2015**, *48*, 4607−4619.
(51) Gumz, H.; Boye, S.; Iyisan, B.; Krönert, V.; Formanek, P.; Voit, B.; Lederer, A.; Appelhans, D. Toward Functional Synthetic Cells: In-Depth Study of Nanoparticle and Enzyme Diffusion through a Cross-Linked Polymersome Membrane. *Adv. Sci.* **2019**, *6*, 1801299.
(52) Kuriyan, J.; Konforti, B.; Wemmer, D. *The Molecules of Life: Physical and Chemical Principles*; W.W. Norton & Company: New York, 2012.
(53) Cooper, C. L.; Dubin, P. L.; Kayitmazer, A. B.; Turksen, S. Polyelectrolyte−protein complexes. *Curr. Opin. Colloid Interface Sci.* **2005**, *10*, 52−78.
(54) Andrianov, A. K.; Chen, J.; Payne, L. G. Preparation of hydrogel microspheres by coacervation of aqueous polyphosphazene solutions. *Biomaterials* **1998**, *19*, 109−115.
(55) Andrianov, A. K.; Chen, J. Polyphosphazene microspheres: Preparation by ionic complexation of phosphazene polyacids with spermine. *J. Appl. Polym. Sci.* **2006**, *101*, 414−419.
(56) Požar, J.; Salopek, J.; Poldrugač, M.; Kovačević, D. The effect of cation type, ionic strength and temperature on the complexation between polyallylammonium cation and polystyrenesulfonate anion. *Colloids Surf., A* **2016**, *510*, 159−168.
(57) Kremer, T.; Kovačević, D.; Salopek, J.; Požar, J. Conditions Leading to Polyelectrolyte Complex Overcharging in Solution: Complexation of Poly(acrylate) Anion with Poly(allylammonium) Cation. *Macromolecules* **2016**, *49*, 8672−8685.
(58) Wang, Q.; Schlenoff, J. B. The Polyelectrolyte Complex/Coacervate Continuum. *Macromolecules* **2014**, *47*, 3108−3116.
(59) Fu, J.; Fares, H. M.; Schlenoff, J. B. Ion-Pairing Strength in Polyelectrolyte Complexes. *Macromolecules* **2017**, *50*, 1066−1074.
(60) Von Ferber, C.; Löwen, H. Complexes of polyelectrolytes and oppositely charged ionic surfactants. *J. Chem. Phys.* **2003**, *118*, 10774−10779.

https://doi.org/10.1021/acspolymersau.3c00006
ACS Polym. Au 2023, 3, 354−364